JOURNAL OF MATERIALS SCIENCE 28 (1993) 1491–1502

Herringbone fracture of a polycarbonate/ABS blend

M.-P. LEE, A. HILTNER*, E. BAER
Department of Macromolecular Science, and Center for Applied Polymer Research, Case Western Reserve University, Cleveland, OH 44106, USA

CHE-I KAO
The Dow Chemical Company, Freeport, TX 77540, USA

Tensile fracture mechanisms in single edge notched injection-moulded specimens of a polycarbonate/ABS 30/70 wt % blend have been studied by fractography. When the tensile force was applied parallel to the injection direction, a herringbone pattern could be observed on the fracture surface, while for the perpendicular case, a reverse herringbone pattern was seen. At the same testing condition, the former was tougher than the latter. Fracture images and two-dimensional temperature profiles in the thickness direction were used to locate the crack initiation sites. Herringbone fracture occurred when the main crack repeatedly interacted with secondary cracks initiated along the centreline. Reverse herringbone fracture was formed in a similar mechanism but secondary cracks initiated near the edge. Anisotropy of the fracture modes was attributed to the processing-induced orientation of the polycarbonate phase near the edge.

1. Introduction

Fractography is widely used in post-failure analysis of metals and glasses where it is generally possible to identify from the appearance of the surfaces where fracture originated, in which direction it propagated and whether it was ductile or brittle. In a previous paper, the fracture surface markings of injection-moulded polycarbonate/ABS blends were described as the composition was systematically varied [1]. Ductile fracture of blends with 10–30 wt % polycarbonate (PC) were characterized by the so-called "chevron" or "herringbone" pattern which has only received passing mention in the plastics literature but has been studied extensively in mild steels [2, 3]. In particular, the characteristic V-shaped ridges pointing towards the origin of the running crack are associated with fracture of mild steel plate. Although the herringbone pattern was widely considered to be indicative of brittle and, therefore, unsatisfactory behaviour in steel ship plate, even more brittle materials such as cast iron and high-alloy tool steel, do not exhibit the herringbone pattern.

It has been pointed out that many times the markings on fracture surfaces, including the herringbone, can best be explained by multiple fracture initiations that propagate and unite to complete separation. The markings owe their visibility to the existence of sharp changes in level and, for this reason, are often called level-difference lines. The herringbone pattern observed in sheet is then a particular case where the concentration of fracture initiation sites is along the centre line. Shearing or tearing along the herringbone ridges, suggesting that the fracture lags or hesitates in the final joining up of the crack fronts, is evidence of plastic deformation before and during fracture [4, 5].

The fracture behaviour of polymers is complicated by flow-induced anisotropy which is a pervasive feature of injection-moulded pieces. Injection moulding of thermoplastics usually produces mouldings with some degree of anisotropy due to orientation of the polymer molecules. When the polymer system is a blend of immiscible phases, injection moulding can produce another type of anisotropy caused by orientation of the phases along melt flow lines. Thus, elongational flow at the melt front produces a skin layer with more or less elongated domains [6–10], while in multiple-gated injection mouldings, blends often exhibit especially weak knit or weld lines [11, 12]. The most dramatic evidence for effects of morphological anisotropy is in the area of fracture phenomena. Anisotropy in the fracture of injection-moulded blends is widespread and in extreme cases the strength of injection mouldings is more related to melt flow patterns than to bulk material properties. It is the purpose of this paper to examine more closely the fracture behaviour of the PC/ABS 30/70 wt % blend and, in particular, to provide an explanation for a herringbone-patterned fracture surface as related to the anisotropic phase morphology.

2. Experimental procedure

A blend of 70% by weight ABS and 30% by weight polycarbonate (PC) was provided in the form of 5 in

* Author to whom all correspondence should be addressed.

0022–2461

(12.7 cm) × 3 in (7.6 cm) × 1/8 in (0.3 cm) plaques. The polymers and injection-moulding conditions were described previously [13]. Tensile specimens were cut to the ASTM-1708 geometry either parallel or perpendicular to the injection direction. These were subsequently referred to as parallel and perpendicular specimens, respectively. A single edge notch (SEN) was machined at the midpoint of the gauge length, the notch was 0.037 in (0.094 cm) in depth with a 0.010 in (0.025 cm) notch radius and 45° flank angle.

Tensile tests were carried out in an Instron machine. The crosshead speed was varied from 0.458–229 mm min^{-1} and the test temperature was varied from − 70–25 °C. In some cases crack propagation in the thickness direction was viewed end-on from either the notched or unnotched end with a Panasonic WV-1800 video camera. In other cases an Inframetrics infrared imaging radiometer was focused on either the notched or the unnotched end of the specimen in order to record temperature changes in the thickness direction during fracture. With the Thermoteknix software from Inframetrics, the data were presented in the form of two-dimensional isothermal contours.

Fracture surfaces were examined with an Olympus Model SZH stereoscan optical microscope in the reflection mode, then coated with gold and viewed in a JEM 35CF scanning electron microscope (SEM). Cross-sectional slices, 0.5 mm thick, were cut with a diamond wafering blade for viewing in the optical microscope.

For morphology studies, parallel and perpendicular tensile specimens were notched and fractured in the Instron at − 70 °C with a crosshead speed of 229 mm min^{-1}. The specimens were cut and notched in such a way that the location of the fracture surfaces corresponded to the midpoint of the plaque. The cryogenic fracture surfaces were subsequently selectively etched by immersion in 30% by weight aqueous potassium hydroxide for 5 h to remove the PC phase, then washed in water for 2 h, dried, coated with gold and examined in the scanning electron microscope [14]. Alternatively, some of the etched specimens were stained with 1 wt % aqueous osmium tetroxide at room temperature for 1 week, then coated with gold and examined in a Jeol 840A scanning electron microscope in the backscattered mode. For transmission electron microscopy, specimen blocks cut from the plaque were stained with 1 wt % aqueous osmium tetroxide for 1 week at room temperature, then sectioned with an RMC MT-6000 ultramicrotome at room temperature. Sections as thin as 60 nm were made in the thickness direction parallel to the injection direction from the region about 0.2–0.7 mm from the edge. Sections were placed on copper grids and viewed in a Jeol 100CX transmission electron microscope.

3. Results and discussion

3.1. Fractography of parallel orientation

SEN specimens of the PC/ABS 30/70 blend were loaded to fracture at various temperatures, − 70–25 °C, and at one temperature − 60 °C with various crosshead speeds, 0.458–229 mm min^{-1}. Typical stress–displacement curves showed significant nonlinearity which usually indicates there is some level of ductility. The maximum stress achieved with specimens cut parallel to the injection direction was in the range of 40–45 MPa. The maximum stress was always lower for specimens cut perpendicular to the injection direction and while there was considerable scatter in this case, no consistent trend with changing temperature was observed. Crack growth began near the maximum stress. Under the mildest testing conditions, room temperature with a crosshead speed of 0.5 mm min^{-1}, fracture was virtually instantaneous for the perpendicular specimens, while the stress–displacement curve of the parallel specimens included a region of decreasing stress during which slow crack propagation occurred.

The markings on the fracture surfaces of parallel specimens tested at temperatures between room temperature and − 20°C were characteristic of the chevron or herringbone pattern that has been described in steel ship plate [2, 3]. Surface markings consisted of a series of ridges that curved outwards from the centre towards the edges, Fig. 1a. When the temperature was decreased to − 25 °C the herringbone pattern did not cover the entire surface, Fig. 1b. The region furthest from the notch took on a featureless appearance with no stress-whitening that was characteristic of fast brittle fracture. The length of the herringbone region decreased as the testing conditions became increasingly severe until at the lowest temperature, − 70 °C, only the crack initiation region was apparent as an area of stress-whitening at the notch in the centre of the fracture surface, Fig. 1c.

Although the herringbone has been identified as a brittle fracture mode, it has also been recognized that some level of plastic deformation occurs in the formation of the ridges [4]. Further evidence that plastic deformation accompanied the herringbone in the PC/ABS blend was provided by visible stress-whitening of the herringbone region when the fracture surface was viewed from above or from the side. A cross-section of the fracture surface showed that the herringbone pattern did not extend to the edges of the fracture surface. When the fracture surface in Fig. 1b was sectioned through the herringbone region about 0.2 cm from the notch and viewed end-on, shear lips were clearly observed near the edges where the stress state approached plane stress. Stress-whitening within the shear lips away from the fracture surface indicated that these regions experienced more plastic deformation than the centre herringbone region.

Early observations on the fracture of steel plate showed that the fracture front at the centre precedes the edges [3, 5]. The same characteristic was seen in the PC/ABS blend when the notch was photographed end-on during testing at − 60 °C with a crosshead speed of 0.5 mm min^{-1}. The final three frames taken 0.03 s apart, showed the notch before fracture initiated, 0.03 s later when fracture had started in the centre, and then at complete fracture. From these photographs the average crack speed in the thickness

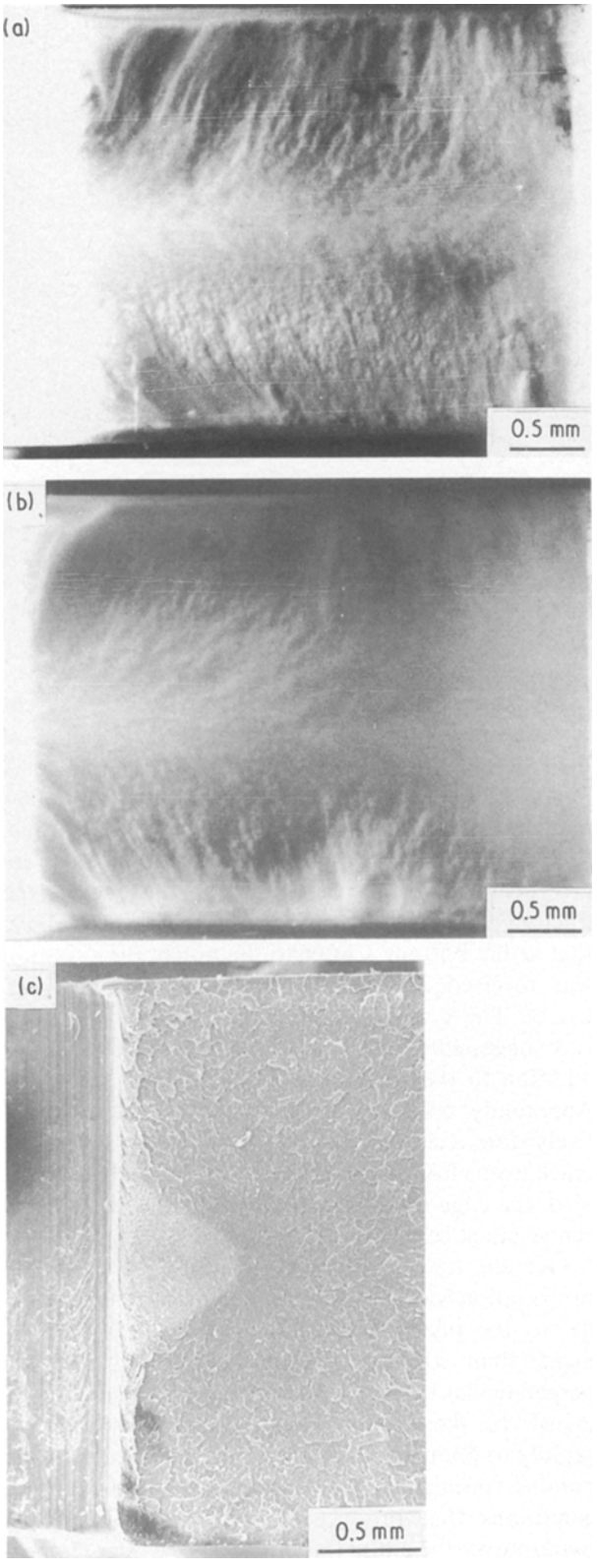

Figure 1 Typical fracture surfaces of parallel specimens tested at a crosshead speed of 229 mm min^{-1} and various temperatures: (a, b) stereoscan optical micrographs at − 20 and − 25 °C, respectively; (c) scanning electron micrograph at − 70 °C. The crack propagated from left to right.

direction in the herringbone region was estimated to be at least 25 mm s^{-1}. A similar experiment was carried out at room temperature with the photographs taken from the unnotched end which was possible in this case because the entire fracture surface was herringbone. The results were the same except that the average crack speed was almost two orders of magnitude slower, approximately 0.4 mm s^{-1}, at the same crosshead speed.

3.2. Fractography of perpendicular orientation

The fracture surface of a perpendicular specimen also showed the ridges of a herringbone pattern but instead

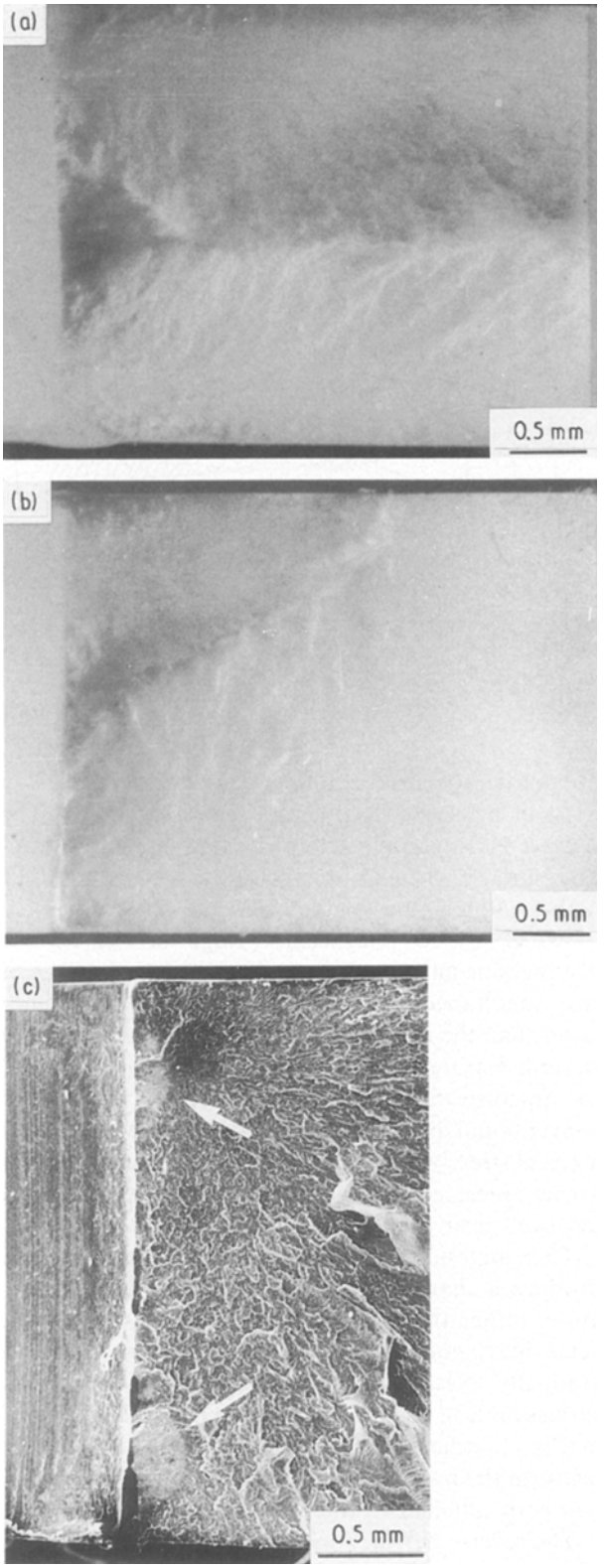

Figure 2 Typical fracture surfaces of perpendicular specimens tested at a crosshead speed of 229 mm min^{-1} and various temperatures: (a, b) stereoscan optical micrographs at − 10 and − 20 °C, respectively; (c) scanning electron micrograph at − 70 °C; the arrows indicate the two locations of crack initiation. The crack propagated from left to right.

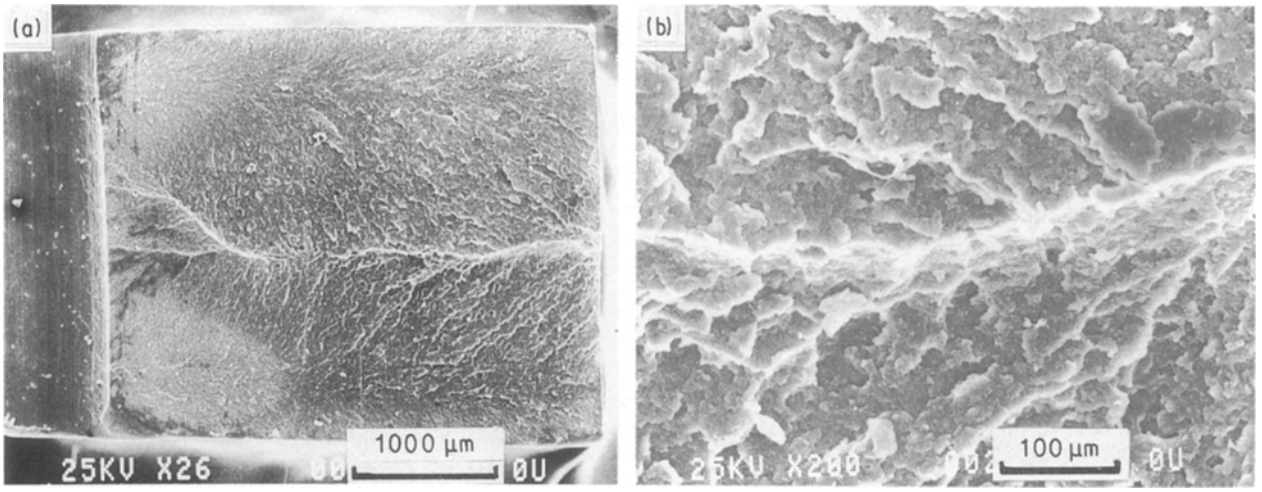

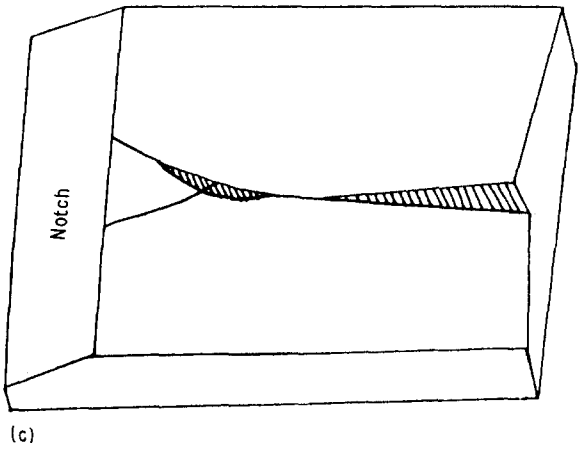

Figure 3 The reverse herringbone pattern: (a) the fracture surface in Fig. 2a of a perpendicular specimen tested at $-10\,^{\circ}C$ with a crosshead speed of 229 mm min^{-1} as viewed in the SEM; (b) a higher magnification of the centre ridge; (c) a schematic representation of the centre ridge.

of pointing toward the notch, the ridges pointed away to form a reverse herringbone pattern, Fig. 2a. The reverse herringbone pattern covered the entire fracture surface when the temperature was $-10\,^{\circ}C$ or higher. When the temperature was decreased to $-20\,^{\circ}C$, the distinct centre ridge of the reverse herringbone curved off towards one edge, as if one of two simultaneous crack fronts had grown slightly faster than the other, and about half the surface had a smooth featureless appearance, Fig. 2b. At $-70\,^{\circ}C$ the fracture surface was characteristic of a more conventional brittle fracture, Fig. 2c, although two areas of stress-whitening at the notch, indicated by the arrows, revealed that crack initiation occurred at two locations near the edges.

This method of notched tensile testing did not produce a sharp ductile-to-brittle transition temperature, rather the transition from herringbone, or reverse herringbone, to fast brittle fracture occurred gradually. Nevertheless, comparison of the fracture surfaces in Fig. 2 with those of the parallel specimens in Fig. 1 indicated that the blend was slightly less brittle in the parallel geometry when the crack growth was perpendicular to the injection direction.

The reverse herringbone pattern has been obtained when side scratches on a cellulose acetate plate induced the fracture to lead from the edges [2]. Evidence that the fracture front proceeded from the edges inward to the centre was obtained by closer examination of the Y-shaped centre ridge. Fig. 3a shows the fracture surface in Fig. 2a viewed in the SEM. The centre ridge was much more prominent than in the stereo-optical micrograph although the ridges and valleys of the reverse herringbone were not as clearly defined. A region of the ridge in Fig. 3a is shown at higher magnification in Fig. 3b. It consisted of an abrupt step, such as would have occurred when cracks that were growing in different planes met. In this region, the fracture plane at the top of the micrograph was above that at the bottom. Closer to the notch, the situation was reversed as shown in the schematic drawing, Fig. 3c. The Y-shape of the centre ridge at the notched end suggested that a crack initiated in the centre in addition to the cracks that initiated near the edges. Apparently, because the initial crack speed was relatively slow, a centre crack had time to start before the crack fronts from the edges met. As the cracks accelerated, the edge cracks dominated while growth of the centre crack ceased.

Overall, fracture was much faster when crack propagation was of the reverse herringbone type parallel to the injection direction (perpendicular specimens) than when it was of the herringbone type perpendicular to the injection direction (parallel specimens). In the former case, fracture occurred too rapidly to photograph by the technique used with the parallel specimens, even with relatively mild testing conditions that produced the reverse herringbone pattern over the entire fracture surface (room temperature and a crosshead speed of 0.5 mm min^{-1}). This meant that the average crack speed in the thickness direction exceeded 50 mm s^{-1}, compared to about 0.4 mm s^{-1} for the parallel specimens under the same conditions. The shear lips were at least partially responsible for the slower crack speed of the parallel specimens. Shear lip formation in the perpendicular specimens was inhibited because crack initiation occurred near the edges.

To confirm the edge initiation of the reverse herringbone in the PC/ABS blends, temperature readings were made from the unnotched end as a specimen was fractured. The infrared temperature profiles

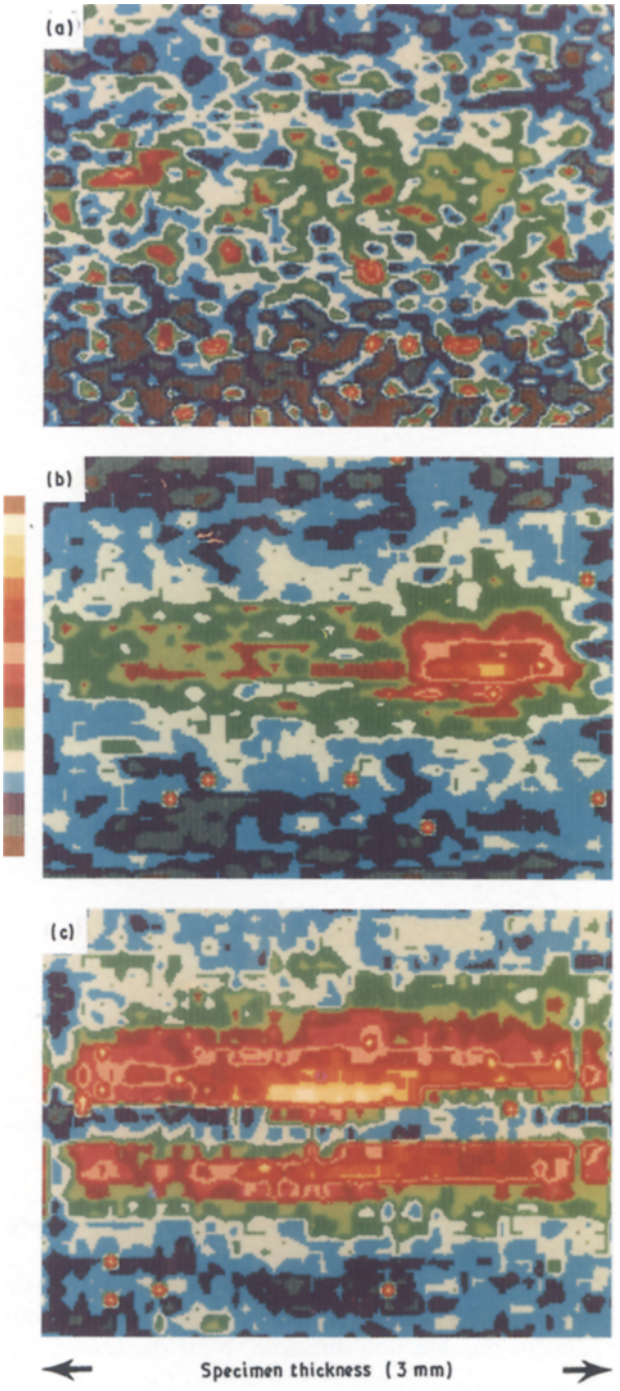

Figure 4 Temperature contours showing fracture of a perpendicular specimen viewed end-on from the unnotched end. Testing was carried out at room temperature with a crosshead speed of 0.5 mm min^{-1}. Each colour level on the scale to the left of the thermogram represents a temperature increment of 0.5 °C: (a) 0.06 s before complete fracture; (b) 0.03 s before complete fracture; (c) fracture.

in Fig. 4 were made at 0.3 s intervals as the specimen fractured, the location of fracture was indicated by a temperature rise over the background. The first two profiles show the specimen during fracture; the edge initiation was confirmed by the location of the highest temperature contours near the left edge in Fig. 4a and the right edge in Fig. 4b. In Fig. 4c, where the specimen had fractured completely, the highest temperature was in the centre which fractured last. The final result was not caused by faster heat loss from the edges for in a similar experiment with a parallel specimen the highest temperature occurred at the edges after fracture.

3.3. Formation of herringbone and reverse herringbone patterns

This description of the fracture process that created the herringbone pattern used the concepts put forward by Boyd [3] in discussing the similar fracture mode in steel plate. The fracture was discontinuous and proceeded by initiation of secondary cracks in front of the primary crack so that impingement of the expanding crack fronts created the characteristic radiating ridges. The formation of one ridge is shown schematically in Fig. 5a. The primary crack initiated at time t_1 and grew radially in all directions. At time t_2 a secondary crack initiated on the centre line in front of the primary crack. It also grew radially at approximately the same speed as the primary crack. If the secondary crack had not grown at a comparable speed, specifically if it had grown more slowly, the main crack would have rapidly overtaken the secondary crack and the pattern of a closed ellipse would have appeared on the fracture surface. The two cracks intersected along a line that extended at an angle outward toward the edge. Because the two cracks grew in slightly different planes, a tearing ridge was formed where they intersected. It has been predicted that the markings should make an angle of 72° with the centre line [3]. In general, the observed angles have agreed quite well with this prediction as was also the case with the PC/ABS blend where the angle was about 68° except near the edges where the shear lips cut off the herringbone pattern.

Sequential crack initiation along the centre line is shown in Fig. 5b. The nth branch of the herringbone markings was formed by the intersection of the nth and $n + 1$th crack fronts initiated at times t_n and t_{n+1}, respectively. If n was large enough and the initiation sites were close enough, the crack front could be considered as a parabolic envelope enclosing many discrete cracks all growing radially. It has been pointed out that in some cases, when a critical crack width is reached, shearing can occur at the edges to create the shear lips that were observed along with the herringbone in the PC/ABS blends [3, 5].

As pointed out above, although the herringbone is sometimes considered a brittle fracture mode, the crack speed was slowed somewhat by a level of plastic deformation. As the test speed was increased or the temperature decreased, this level of ductility was lost and the crack speed increased until it was too fast for secondary cracks to initiate and grow. The critical point was identified on the fracture surfaces by the transition from the herringbone to the markings of a parabolic crack front. The location of this transition moved closer to the notch as the test conditions became more severe.

Formation of the reverse herringbone pattern occurred by a similar mechanism except that the multiple initiation sites occurred near the edges of the specimen. Fig. 6a shows schematically how the primary and secondary cracks impinged to produce a

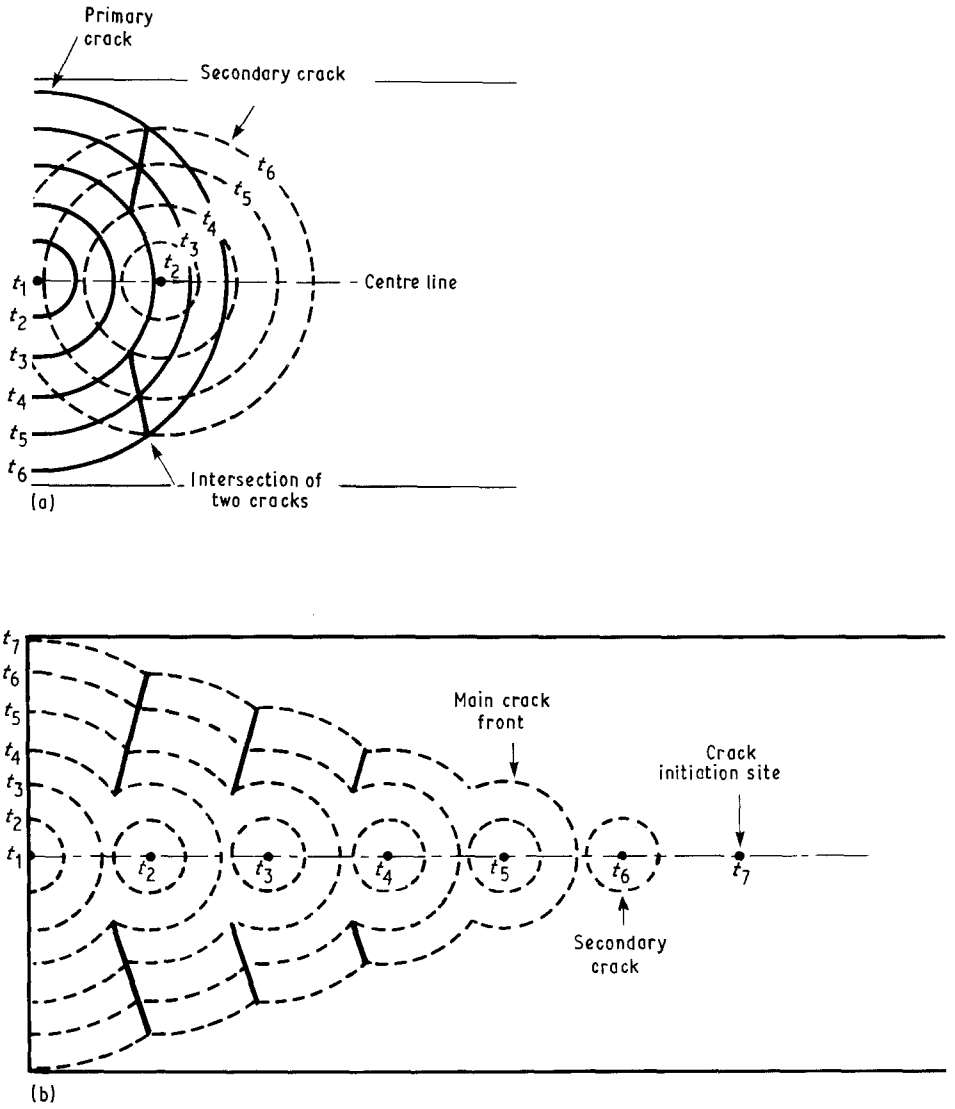

Figure 5 Proposed mechanism for formation of the herringbone pattern: (a) schematic representation of formation of one pair of radial markings; (b) schematic illustration of the formation of the herringbone pattern.

radial ridge of the reverse herringbone. In this case, the crack front could be considered a combination of the opposite halves of two parabolic crack fronts, Fig. 6b. The centre ridge was formed where the two crack fronts, which might have been growing in slightly different planes, met. When the initiation time was insignificant compared to the overall crack speed, simultaneous growth of two crack fronts produced a symmetrical reverse herringbone pattern. However, when the temperature decreased into the ductile-to-brittle transition region and the crack speed correspondingly increased, the reverse herringbone became asymmetric as in Fig. 2b if the two cracks initiated at slightly different times or if one crack propagated slightly faster than the other.

3.4. Morphology

Typical unetched cryogenic fracture surfaces from the middle of the plaque show views parallel to the injection direction from the centre and near the edge, Fig. 7a and b. In the centre the PC formed more or less spherical domains about 1 μm or less in diameter, while near the edge the PC domains were highly elongated in the injection direction. It was apparent in the micrographs that some separation of the phases occurred during fracture.

The etched surfaces from four positions through the thickness in Fig. 8 show views parallel and perpendicular to the injection direction. Near the centre, Fig. 8a and b, the morphology appeared the same in the two directions with spherical holes where the PC domains were etched away. The holes were the same size, 1 μm or less, as the spherical domains in Fig. 7a. At a position almost half-way between the centre and edge, Fig. 8c and d, the morphology was similar to that observed in the centre; the PC domains were the same size as in the centre and the shape was generally spherical although especially in the parallel view, Fig. 8c, a few of the PC domains were slightly elongated in the injection direction. Closer to the edge, the holes that revealed the size and shape of the PC domains were thinner and elongated in the injection direction. This was particularly apparent in the view parallel to the injection direction, Fig. 8e. When viewed perpendicular to the injection direction, Fig. 8f, the PC domains appeared from the shape of the holes to be more or less circular in cross-section, the diameter of the holes was smaller than in the centre and corresponded to the width of the elongated holes in

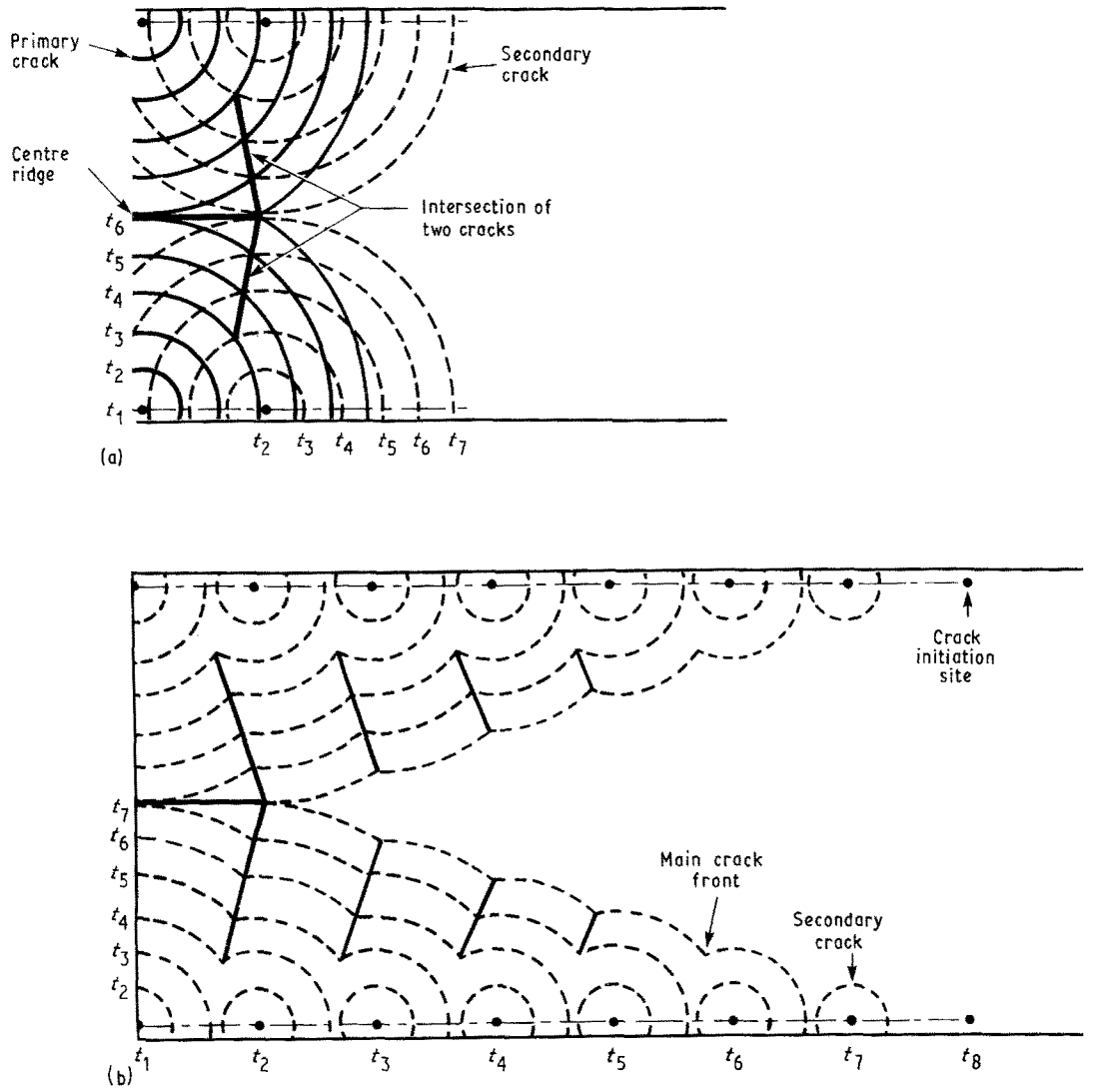

Figure 6 Proposed mechanism for formation of the reverse herringbone pattern: (a) schematic representation of formation of one pair of radial markings; (b) schematic illustration of formation of the reverse herringbone pattern.

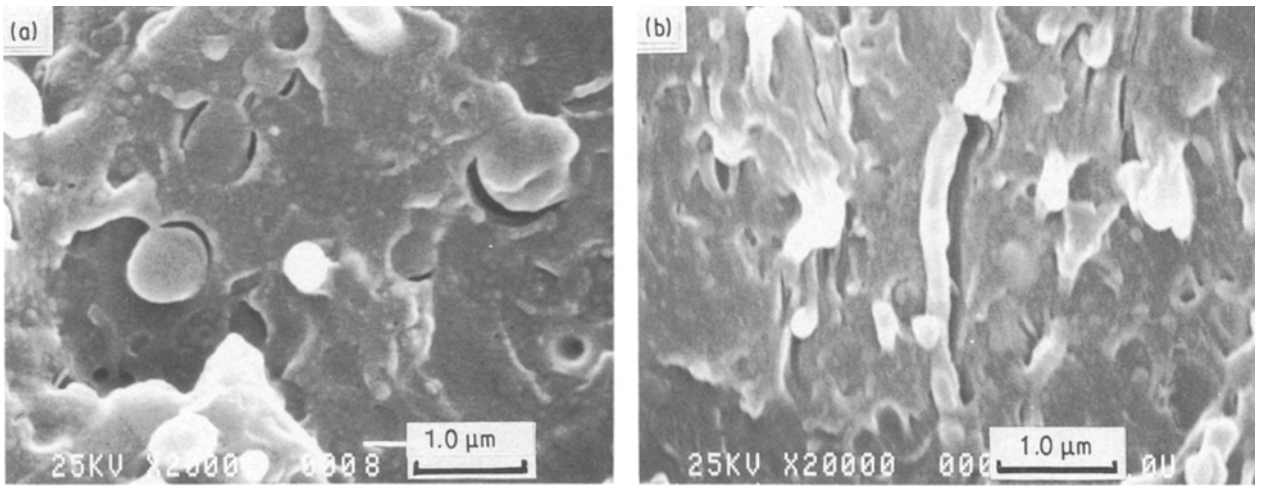

Figure 7 Scanning electron micrographs of the unetched fracture surface of a perpendicular specimen tested at $-70\,^{\circ}C$ with a crosshead speed of 229 mm min^{-1}: (a) a region in the centre, and (b) a region near the edge. The injection direction was from top to bottom.

the parallel view. In this region of the plaque it appeared that the PC domains were predominantly fibrillar or rod-shaped and oriented in the injection direction. The parallel view closest to the edge showed some increase in the length of the PC domains, Fig. 8g. In the corresponding perpendicular view, Fig. 8h, some of the holes were also elongated which suggested that close to the edge the PC domains were lamellar or sheet-like as well as rod-shaped. Not shown in the micrographs was a featureless outer layer that extended less than 0.1 mm inward from the edge. Although in this region no domain morphology on the

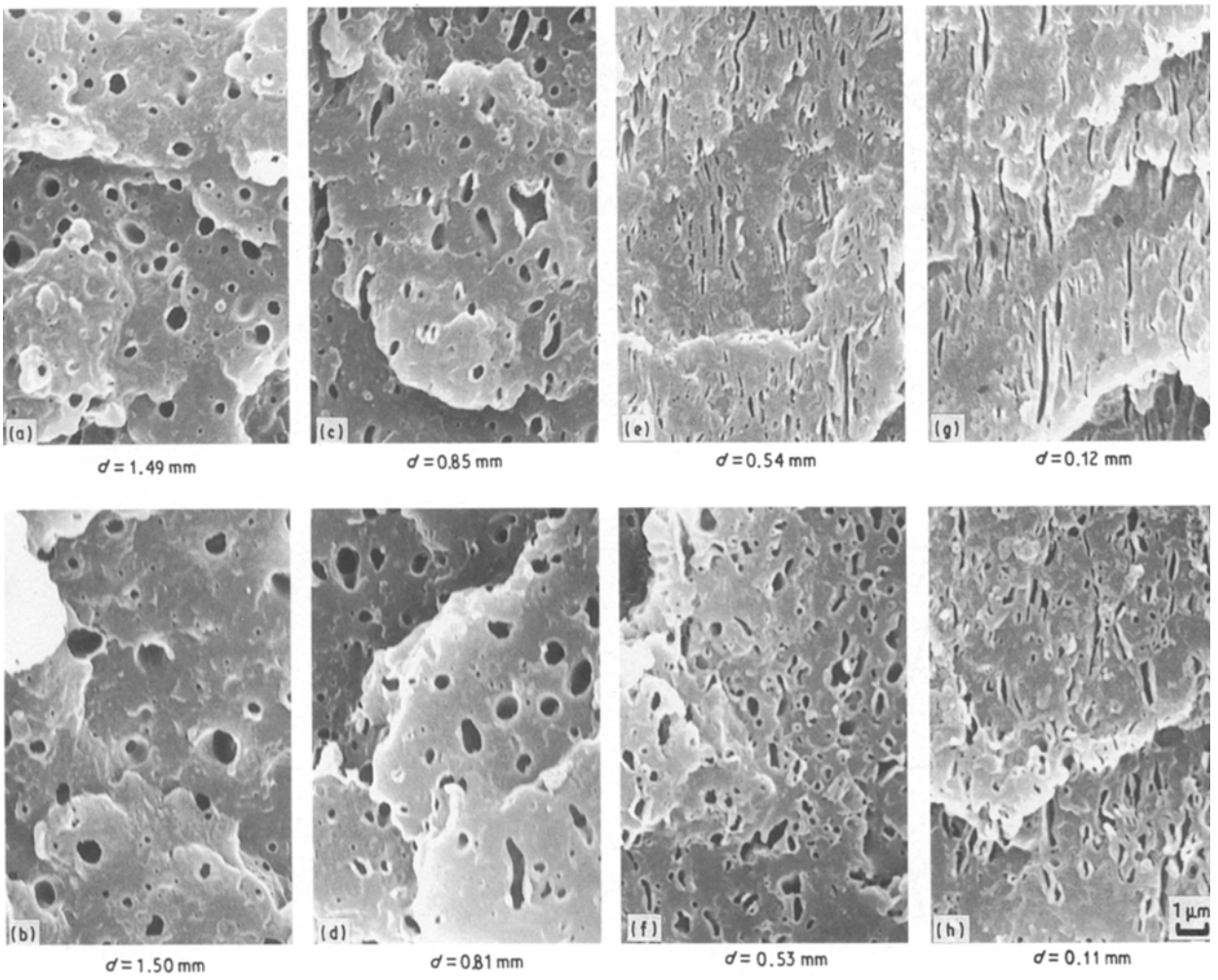

Figure 8 Scanning electron micrographs of etched cryogenic fracture surfaces at various positions through the thickness: (a, c, e, g) parallel to the injection direction; (b, d, f, h) perpendicular to the injection direction. The distance, *d*, from the edge of the 3 mm thick plaque is indicated with each micrograph.

micrometer size scale was revealed by etching the fracture surfaces, when the mould-contacting surface of the plaque was etched, very long, thin rod-shaped domains of PC about 0.05 µm or less in diameter were observed, Fig. 9.

A three-dimensional model of the PC morphology, Fig. 10, was constructed from the morphological observations. It shows the more-or-less isotropic morphology in the centre region with spherical PC domains 1 µm or less in diameter dispersed in the ABS matrix. Towards the edge the PC domains became elongated in the injection direction and close to the edge took on a rod-like or sheet-like shape. This model is similar to that described for injection-moulded polypropylene blends [6] although the distinct gradient in concentration of the dispersed phase

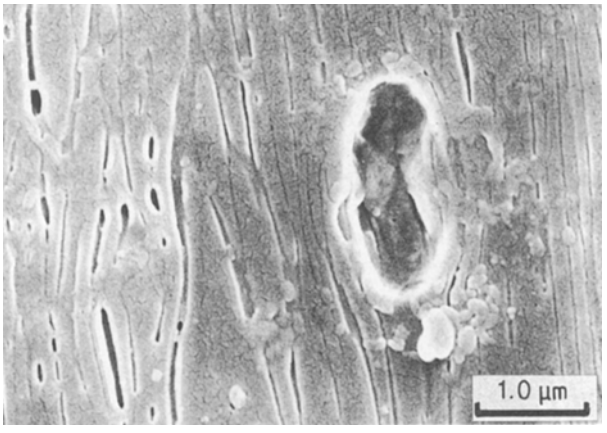

Figure 9 Scanning electron micrograph of etched mould-contacting surface. The injection direction was from top to bottom.

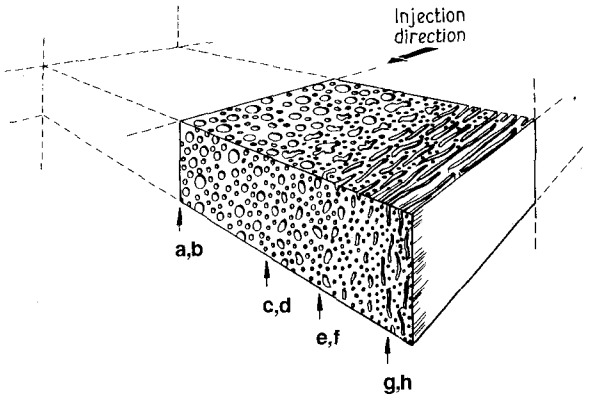

Figure 10 Schematic representation of the morphology. The positions of the micrographs in Fig. 8 are indicated.

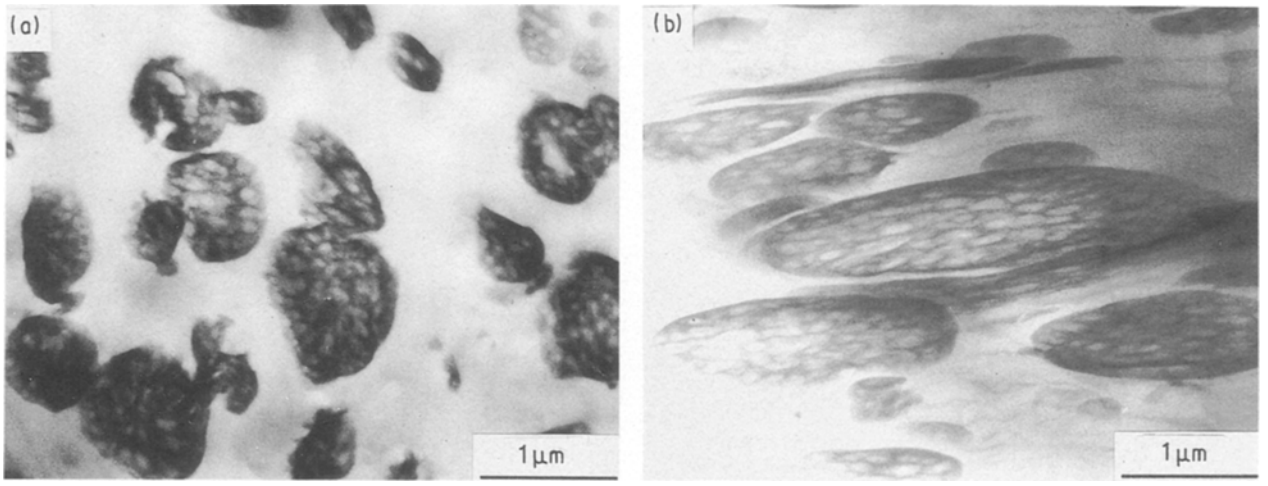

Figure 11 Transmission electron micrographs of OsO_4-stained sections: (a) from the centre; (b) near the edge. The injection direction was from left to right.

through the thickness of the polypropylene blend was not readily apparent in the PC/ABS blend.

The ABS phase itself was heterogeneous; the composite rubber particles were evident in stained sections viewed in the transmission electron microscope, Fig. 11a. Only composite particles were observed, these were fairly uniform in size with a diameter of about 0.7–1 μm. Very near the edge, the rubber particles were slightly elongated, Fig. 11b. The size and shape of the rubber particles at various locations through the thickness were determined by viewing OsO_4-stained cryogenic fracture surfaces in the SEM in the backscattered mode. Only in a very narrow region that extended about 50 μm inward from the edge, were the rubber particles slightly elongated in the injection direction; through the remainder of the plaque thickness the rubber particles were spherical.

The length-to-width ratio of the PC domains and the composite rubber particles, Fig. 12, shows the change in shape through the thickness at the midpoint of the plaque. There was a very thin skin region of about 50 μm where the PC domains had, on average, a very high aspect ratio and the rubber particles were also elongated. In the fountain flow pattern, elongational flow perpendicular to the injection direction carries material from the centre of the melt front to the mould surface where it solidifies rapidly to form this characteristic skin layer. Cross-linking in the rubber particles prevented them from being more extended, but the PC domains were highly drawn under the elongational flow at the melt front. Behind the melt front, the PC domains were elongated by shear and elongational flow prior to entering the mould and by shear flow in the mould. The gradient in aspect ratio through the plaque depended on the shear rate profile through the thickness, which determined the amount of elongation in the melt, and the cooling rate after mould filling, which controlled the amount of melt relaxation from rod-shaped to spherical domains before solidification. Under the processing conditions used in this study, these factors produced a region that extended from the skin about 0.7 mm or half-way to the centre where the PC domains were elongated in the injection direction with an aspect ratio in the range 12–15; in this region, the rubber particles were spherical. The morphology in the centre half of the thickness was isotropic with spherical PC domains.

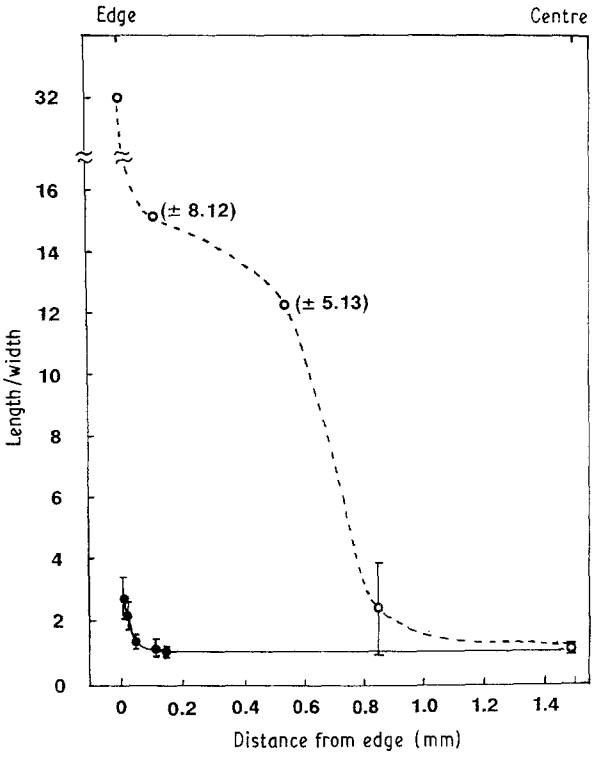

Figure 12 The length-to-width ratio of the PC domains (○) and the rubber particles (●) through the thickness of the 3 mm thick plaque at its midpoint.

3.5. Microstructure of fracture surfaces

Deformation at the size scale of the domains in this compatible blend was observed when fracture surfaces were viewed at higher magnification in the SEM. The fracture surface of the parallel specimen tested at $-25\,^{\circ}C$ with a crosshead speed of 229 mm min^{-1} in Fig. 1b had a herringbone region adjacent to the notch and further away from the notch, a featureless region

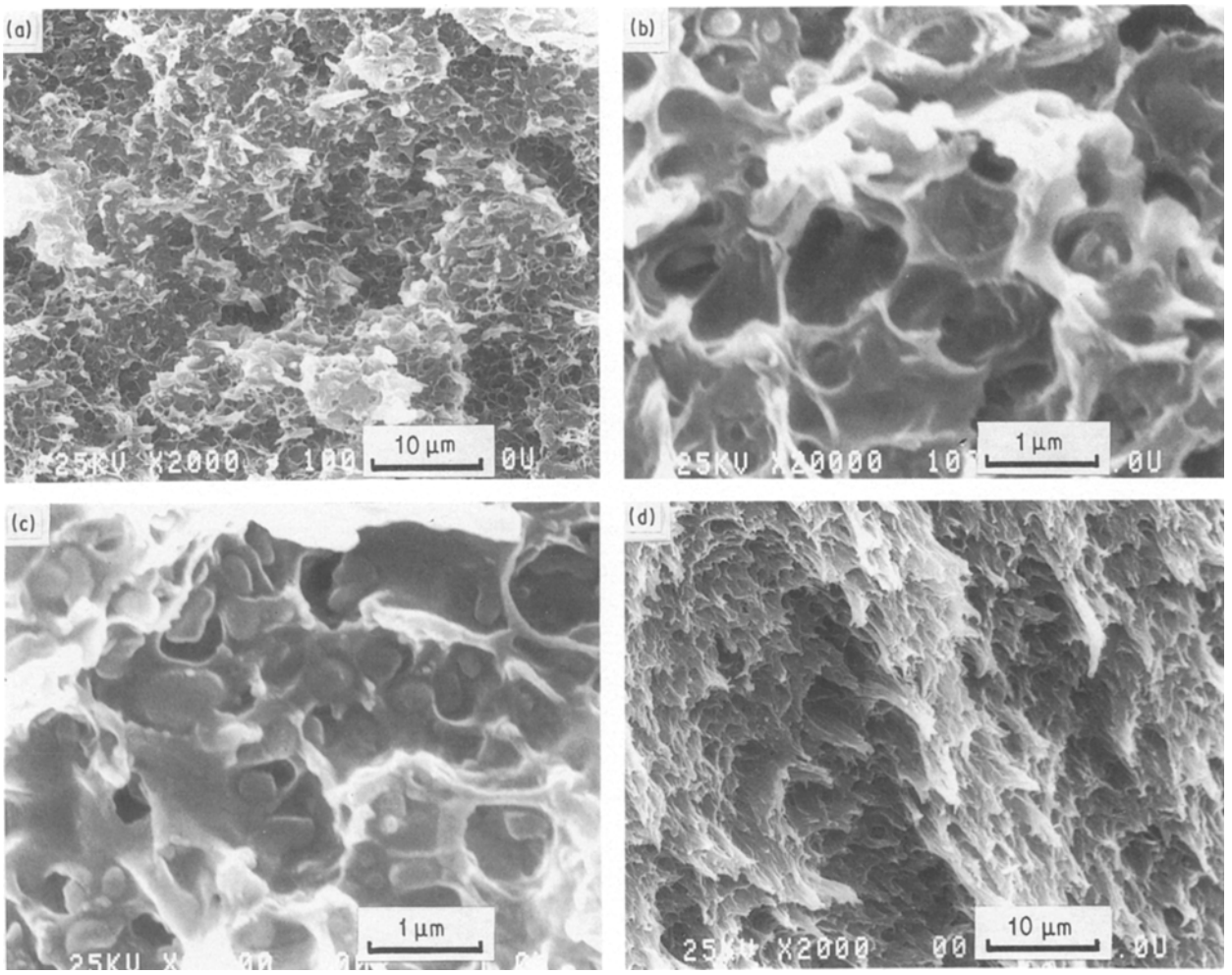

Figure 13 Scanning electron micrographs showing various regions of the fracture surface in Fig. 1b, a parallel specimen tested at $-25\,^{\circ}C$ with a crosshead speed of 229 mm min^{-1}: (a) the centre region of the herringbone; (b, c) higher magnifications of (a); (d) a radial ridge in the outer portion of the herringbone. The crack propagated from left to right.

of brittle fracture. The brittle region was indistinguishable from the $-70\,^{\circ}C$ fracture surface that showed the undeformed domain morphology, including occasional separation of the PC particles from the ABS continuous phase (cf. Fig. 7a and b). At higher magnification, undeformed composite rubber particles of the ABS were also discernible.

In the ductile region closer to the notch, a view of the multiple crack initiation zone at the centre of the herringbone region, Fig. 13a, revealed spherical cavitated rubber particles, Fig. 13b, as well as cavitation of the matrix around the PC domains, Fig. 13c. In this view, the plastically deformed matrix was not adhered to the PC particles which retained their more or less spherical shape. A radial ridge of the herringbone away from the initiation zone, Fig. 13d, showed obliquely slanted peaks characteristic of shear or tear failure [15]. In general, the rubber particles were obscured by the pulled-out ABS and only occasionally was a cavitated rubber particle visible that had been pulled along the tear direction.

The domain morphology was essentially isotropic in the centre, so similar triaxial stress conditions would have been required to initiate a crack in the centre regardless of whether the specimen orientation was parallel or perpendicular. The consistently lower failure stress of the perpendicular specimens suggested that fracture initiated at a weaker site before the required conditions were achieved at the centre. The perpendicular fracture surface obtained at $-70\,^{\circ}C$, Fig. 2c, had two small stress-whitened regions about 0.45 mm inward from the edges that marked the fracture initiation sites. The stress-whitening was produced by profuse cavitation, Fig. 14a; the pulled-out tufts of material were identified as ABS because they were not removed by etching. Cavitated rubber particles were seen in this region at higher magnification, Fig. 14b, and in addition, rod-shaped holes that corresponded in size and shape to the PC domains suggested that interfacial separation had occurred. This specimen had an otherwise featureless brittle fracture surface.

An example of a ductile fracture where the entire fracture surface was the reverse herringbone was the perpendicular specimen tested at $-10\,^{\circ}C$ and a crosshead speed of 229 mm min^{-1} shown in Fig. 3a. This fracture surface also had two stress-whitened regions near the edges where cracks initiated, but in this case they were somewhat larger. Higher magnification showed essentially the same features as the crack initiation region of the $-70\,^{\circ}C$ fracture surface (cf. Fig. 14a and b). The plastic deformation did not extend into the crack propagation region of the reverse herringbone. When the ridges of the reverse

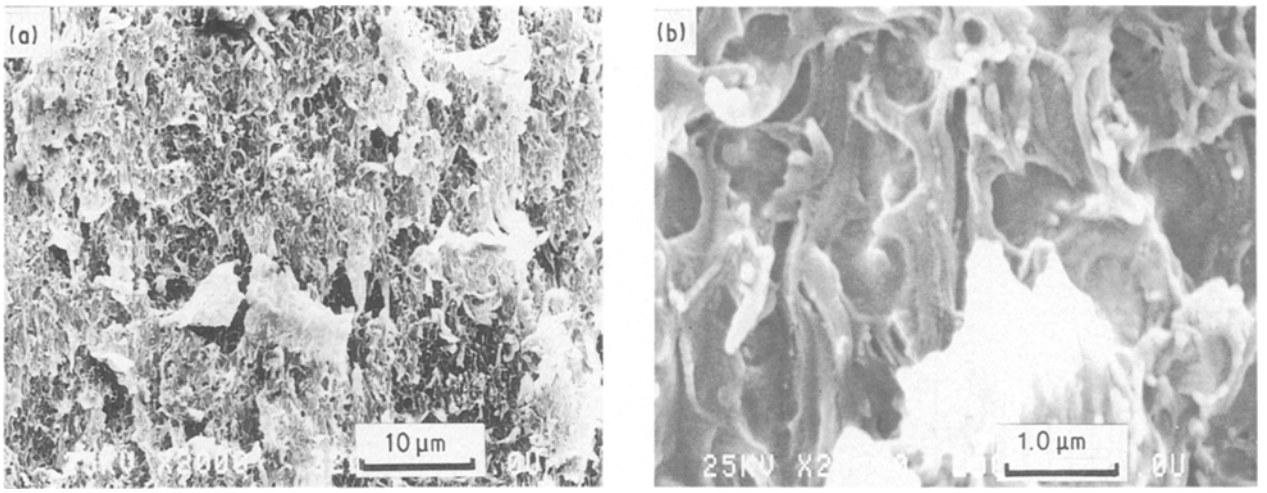

Figure 14 Scanning electron micrographs of the fracture surface in Fig. 2c, a perpendicular specimen tested at $-70\,^{\circ}C$ with a crosshead speed of 229 mm min^{-1}: (a) the crack initiation region near the edge; (b) a higher magnification of (a). Both the crack propagation direction and the injection direction were from top to bottom.

herringbone were viewed at higher magnification their appearance at the size scale of the domain morphology was indistinguishable from the brittle fracture surface (cf. Fig. 7a) with undeformed rubber particles and some separation of the undeformed PC domains.

Because fracture would not have initiated at this unusual site in an isotropic material, some feature of the anisotropic domain morphology resulted in weakness in the perpendicular orientation near the edges that caused premature crack initiation at this location. The major anisotropic feature of these blends was the morphology of the PC domains especially toward the edges where they were elongated in the injection direction. The relationship of the morphology to the crack plane and fracture surface markings is shown schematically in Fig. 15 for the two orientations. In the parallel specimens, the crack initiated in the centre and grew toward the edge where it encountered elongated PC domains oriented perpendicular to the advancing crack front; while in the perpendicular specimens the crack initiated near the edges in the plane of the elongated PC domains and propagated towards the centre to create the reverse herringbone.

It was suggested previously [1] that the herringbone fracture of parallel PC/ABS 30/70 specimens proceeded initially with crazing of SAN and cavitation of rubber particles (R) in the centre where the triaxiality was highest. When the growing craze encountered a PC domain, it created a local stress concentration at the interface. In this blend composition, the PC domains were not continuous and all the load carried by the PC domains was transferred across the interface from the ABS phase. It was apparent from the ductile fracture surfaces, specifically the presence of voids containing undeformed spherical PC particles, that adhesion was not strong enough to support drawing of the PC domains, and instead the interface failed during craze growth as shown schematically in Fig. 16a. Initiation of secondary cracks from the resulting voids would account for the multiple crack initiation that was characteristic of herringbone fracture.

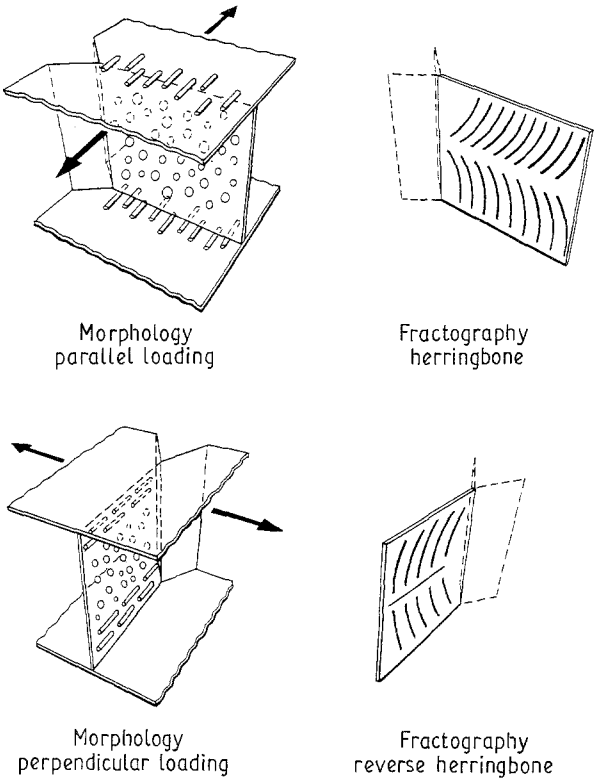

Figure 15 Schematic representation showing how the anisotropic morphology produced the herringbone and reverse herringbone fractures. The arrows indicate the tensile loading direction.

As the crack propagated from the initiation site in the centre toward the edge, it encountered the region where elongated PC domains were oriented perpendicular to the advancing crack front. This had a crack blunting effect [16]. Transfer of the applied load became more efficient when the shape of the PC domains changed from spherical to elongated in the loading direction. Impingement of the craze at the crack tip on an elongated PC domain is shown schematically in Fig. 16b. It was possible that some plastic deformation of the PC phase might have occurred before the interface failed completely, although this could not be confirmed because the PC domains were

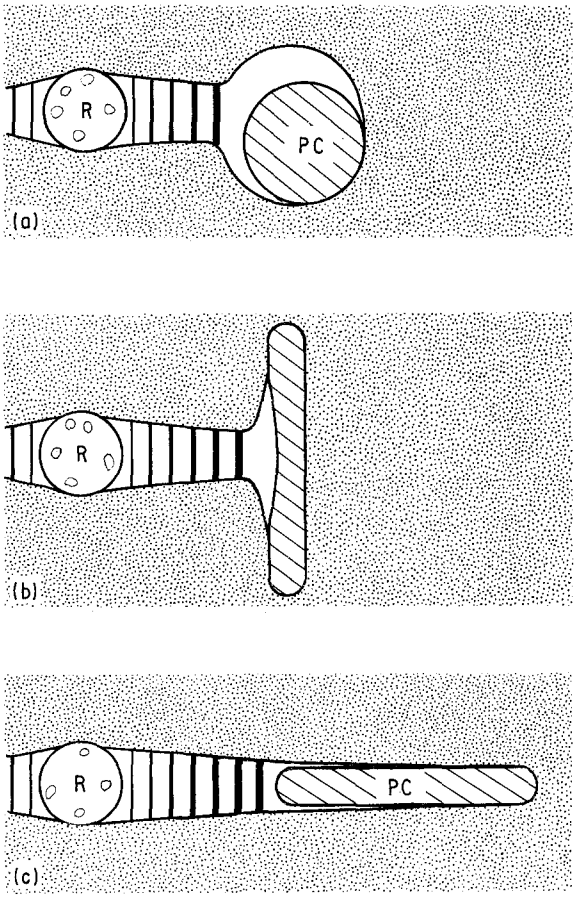

Figure 16 Schematic representations of craze growth; (a) growth of a craze in the centre region; (b) growth of a craze near the edge in herringbone fracture; (c) growth of a craze near the edge in reverse herringbone fracture.

obscured from view in the SEM by the pulled-out ABS phase. Even after failure of the interface, pullout of the PC domains would have retarded the crack growth. The crack was further slowed by formation of shear lips as the condition approached plane stress near the edges.

The initial deformation preceeding reverse herringbone fracture was also thought to be cavitation of rubber particles and craze formation in the SAN at the crack initiation site. However, in this case, the fracture plane was parallel to the injection direction and when the craze encountered a PC domain, as shown schematically in Fig. 16c, failure of the interface created large rod-shaped voids that were visible on the fracture surface at the crack initiation site. Rather than crack blunters, the elongated PC domains in this orientation acted as crack enhancers. Although the elongated shape of the PC domains facilitated crack initiation and growth in the perpendicular orientation, the location of crack initiation was not where the PC domains had the highest aspect ratio, which was near the mould surface, but approximately 0.45 mm inward from the edge where the triaxial condition increased the tendency towards cavitation.

The rough estimates of crack speed indicated that propagation was much faster when the crack initiated near the edge in the perpendicular specimens than when the crack initiated in the centre in the parallel specimens, and this was confirmed by the appearance of the fracture surfaces. While the crack initiation regions showed cavitation and plastic deformation of the matrix in both cases, comparison of the ridges and valley of the herringbone and reverse herringbone clearly revealed that a ductile tearing mode produced the ridges and valleys of the herringbone, while those of the reverse herringbone had the appearance of brittle fracture which meant that the rate of crack propagation in this case exceeded the time scale of cavitation and ductile tearing.

4. Conclusions

A fractographic and morphological study led to the following conclusions regarding the fracture of an injection-moulded PC/ABS 30/70 blend.

1. Fracture occurred by a herringbone mechanism perpendicular to the injection direction and by a reverse herringbone mechanism when fracture occurred parallel to the injection direction. The blend was somewhat less tough in the latter configuration.

2. The herringbone pattern arose from interaction of the main crack with secondary cracks initiated along the centre line. Reverse herringbone fracture occurred by a similar mechanism but crack initiation occurred near the edges.

3. Directional differences in the fracture behaviour were attributed to the processing-induced orientation of the PC phase near the edge.

Acknowledgements

This work was generously supported by The Dow Chemical Company and the National Science Foundation, Polymers Program (DMR 87-13041).

References

1. M.-P. LEE, A. HILTNER and E. BAER, *Polym. Engng Sci.*
2. J. A. KIES, A. M. SULLIVAN and G. R. IRWIN, *J. Appl. Phys.* **21** (1950) 716.
3. G. M. BOYD, *Engineering* **175** (1953) 65, 100.
4. C. F. TIPPER, *J. Iron Steel Inst.* **185** (1957) 4.
5. *Idem, Met. Rev.* **2** (1957) 195.
6. J. KARGER-KOCSIS and I. CSIKAI, *Polym. Engng Sci.* **27** (1987) 241.
7. K. KATO, *Polymer* **8** (1967) 33.
8. *Idem, ibid.* **9** (1968) 225.
9. L. H. HENRY, *Polym. Engng Sci.* **14** (1974) 167.
10. S. KOIWA, *J. Appl. Polym. Sci.* **19** (1975) 1625.
11. E. M. HAGERMAN, *Plast. Engng* **50** (1973) 67.
12. R. C. THAMM, *Rubber Chem. Tech.* **50** (1977) 24.
13. M.-P. LEE, A. HILTNER and E. BAER, *Polymer* in press.
14. G. C. EASTMAN and E. G. SMITH, *ibid.* **14** (1973) 509.
15. L. ENGEL, H. KLINGELE, G. W. EHRENSTEIN and H. SCHAPER, "An Atlas of Polymer Damage" (Prentice-Hall, Englewood Cliffs, NJ, 1992) p. 147.
16. J. COOK and J. E. GORDON, *Proc. R. Soc. Lond. A* **282** (1964) 508.

Received 7 August
and accepted 10 September 1991